Global and Planetary Change 111 (2013) 31–42

Contents lists available at ScienceDirect

Global and Planetary Change

journal homepage: www.elsevier.com/locate/gloplacha

Cold air intrusions over southeastern South America — GFDL model behavior regarding climate simulations in the 20th century and future projections

Iracema F.A. Cavalcanti [a,*], Gabriela V. Müller [b], Kelen M. Andrade [a], Maria Elena Fernández Long [c]

[a] Centro de Previsão de Tempo e Estudos Climáticos/Instituto Nacional de Pesquisas Espaciais (CPTEC-INPE), Brazil
[b] Centro de Investigaciones Científicas y Transferencia de Tecnología a la Producción (CICYTTP-CONICET), Diamante, Argentina
[c] Facultad de Agronomía, Cátedra de Climatología y Fenología Agrícolas, Universidad de Buenos Aires (UBA), Argentina

ARTICLE INFO

Article history:
Received 18 March 2013
Received in revised form 9 August 2013
Accepted 11 August 2013
Available online 20 August 2013

Keywords:
cold air intrusion
temperature changes in South America
CMIP3-GFDL-CM2.0
atmospheric features
future projections
temperature extremes

ABSTRACT

Cold air intrusions in three areas frequently affected by frosts of southeastern South America are analyzed based on GFDL-CM2.0 Coupled Atmospheric and Oceanic Global Circulation Model. The general objective is to investigate the model ability to simulate the frequency of intrusions in the present climate as well as the changes in the frequency of occurrence and atmospheric characteristics in a future climate scenario. The cold period (May to September) is analyzed for the control period 1961 to 1990 and for the period 2081 to 2100 from the CMIP3 A2 scenario, which reflects the extreme global warming. The coupled GFDL-CM2.0 overestimated the number of cold air intrusions for the present climate (control). This systematic error should be considered in the analyses of future climate results. Future projections indicated a reduction of these cases in GFDL results. As this model overestimated the number of cases, the reduction could be even greater. Composites of extreme cases for the present and future climate in the three areas indicated intensification of the temperature gradient which suggests more vigorous frontal systems, intensification of post-frontal highs and cold air extending to lower latitudes as compared to the present climate. Anomaly intensification was related to the climatological mean temperature, which is higher in the future than in the present. Therefore, even with less cold air intrusion over southeastern South America and a lower number of frost cases in the three areas, the occurrence of more intense systems would have an impact on the agriculture of these areas and such impact would extend to lower latitudes.

1. Introduction

Even though an increase in both minimum temperature and number of warm nights as well as a reduction of cold nights number have been registered in the last years over several regions of South America (Vincent et al., 2005; Alexander et al., 2006; Haylock et al., 2006; Barrucand et al., 2008; Marengo et al., 2010; Rusticucci et al., 2010), extreme events of cold air intrusion have also been reported after the passage of cold fronts over the continent. These specific events have affected the agriculture and economy of southern countries in southeastern South America: Argentina, Uruguay, Paraguay and Brazil. Even with the global temperature rise (IPCC, 2007) at high latitudes, reducing the north–south temperature gradient that affects the atmospheric baroclinicity, the synoptic systems could be more intense in a more energetic atmosphere. Trenberth (1999) discussed the role of global warming on the hydrological cycle as well as on the increase of moisture in the atmosphere to feed the systems. Hall et al. (1994) noticed a poleward displacement of the Northern Hemisphere storm tracks and intensification of transient systems in a general circulation model experiment with an increase in CO_2. Other experiments using Global Circulation Models forced by greenhouse gases also led to a poleward shift and an increase in intensity of the storm tracks (Kushner et al., 2001; Yin, 2005).

The Special Report on Extremes (SREX, 2012) provided a global review and assessment of the relationship between climate extremes, their impact and the strategies to manage associated dangers. Studies on extreme events in several regions of the globe have reflected a reduction in extreme events of cold days and few cases of frosts in observed data and future scenarios (Meehl et al., 2000; Easterling et al., 2000;

* Corresponding author at: CPTEC/INPE, Rodovia Presidente Dutra, Km 40, Cachoeira Paulista, São Paulo, Brazil.
E-mail addresses: iracema@cptec.inpe.br (I.F.A. Cavalcanti), gabrielamuller@cicyttp.org.ar (G.V. Müller), kelen.andrade@cptec.inpe.br (K.M. Andrade), flong@agro.uba.ar (M.E. Fernández Long).

0921-8181/$ – see front matter © 2013 Elsevier B.V. All rights reserved.
http://dx.doi.org/10.1016/j.gloplacha.2013.08.006

Alexander et al., 2005). Similar results were reported in different countries, such as a reduction in the annual number of frost days in Canada (Bonsal et al., 2001) and in the United States of America (Easterling, 2002), and a reduction of 5 to 15 frost days in the period running from 1951 to 1998 in New Zealand (Salinger and Griffiths, 2001). During 1951–2000, the frost-free period increased around 0.5 day/year in Germany, Austria and Switzerland and 0.34 day/year in Estonia (Menzel et al., 2003). A reduction in frost occurrences in the Pampa region (central-northern Argentina) during 1964 to 2003 was observed by Fernández Long and Müller (2006) and the shortening of frost periods during the total period 1940–2007 was discussed in Fernandez Long et al. (2013).

Andrade et al. (2012) indicated that the synoptic characteristics of frontal systems in South America had been well simulated in the present climate by two models, GFDL and HadCM3 from CMIP3. However, the model simulations overestimated the frequency of frontal occurrence in southeastern regions in the observed period. Skansi et al. (2013) revealed the results of an assessment of changes in both area-averaged and station-based climate extreme indices over South America for the last half of the twentieth century using high-quality daily maximum and minimum temperature series. They reported strong warming evidence in South America with cold (warm) extremes decreasing (increasing) over the 1950–2010 period. Southeastern South America has been more intensively explored for observed changes in temperature extremes during the last half of the twentieth century (Rusticucci et al., 2010 in Argentina; Rusticucci and Renom, 2008 in Uruguay; Marengo and Camargo, 2008 in southern Brazil), and for model simulations of annual indices of extreme temperature climate events (Marengo et al., 2010; Rusticucci et al., 2010). A positive trend in night time temperatures observed in station data of South America was well represented by CMIP3 models (Marengo et al., 2010). Rusticucci et al. (2010) simulated annual indices of extreme temperature climate events in South America during the last half of the twentieth century, and showed that the number of warm nights is better represented by models than frost days.

The agricultural areas in southeastern regions of South America are frequently affected by frosts in the cold months. Based on the negative trend in cold nights as seen in recent publications of climate change in the region, a question that arises is: can we expect fewer cold air intrusions in the future, and what would be the associated atmospheric conditions? Therefore, the objective of this study is to identify the occurrence of cold air cases over specific areas of southeastern South America, which are frequently affected by frosts. The results from model simulations are compared to observations conducted during a period in the 20th century, to further investigate the changes in frequency and intensity of cases in the future climate. The observed cases are not expected to be represented in the simulations, still it is worth verifying if the models have the ability to represent the frequency of cases during the period, and whether the number of cases are over or underestimated. The evaluation of the models' behavior in the areas frequently affected by frosts and the identification of changes in this behavior are issues worth addressing so as to be aware of the models' limitations and the degree of reliability of the results, as well as to alert about future changes.

2. Data and methods

Three areas comprising Brazil, Uruguay, Paraguay and Argentina were selected, with 5° lat × 5° lon: area 1 (52°W–57°W, 23°S–28°S), area 2 (52°W–57°W, 28°S–33°S) and area 3 (65°W–60°W, 33°S–38°S) (Fig. 1). These represent areas of frost risk in regions of large agricultural production in southeastern South America. The observed daily mean temperatures in those areas were obtained from the National Meteorological Service (Argentina), the National Meteorological Direction (Uruguay), the Hydrological and Meteorological Direction (Uruguay), and CLARIS data (Tencer et al., 2011). The surface temperature at station data was compared to the NCEP/NCAR 925 hPa reanalysis data (Kalnay et al., 1996) in the period available for each area using the meteorological station data of the three areas above particularized. The analyses of the 20th century period ranged from May to September 1961 to 1990.

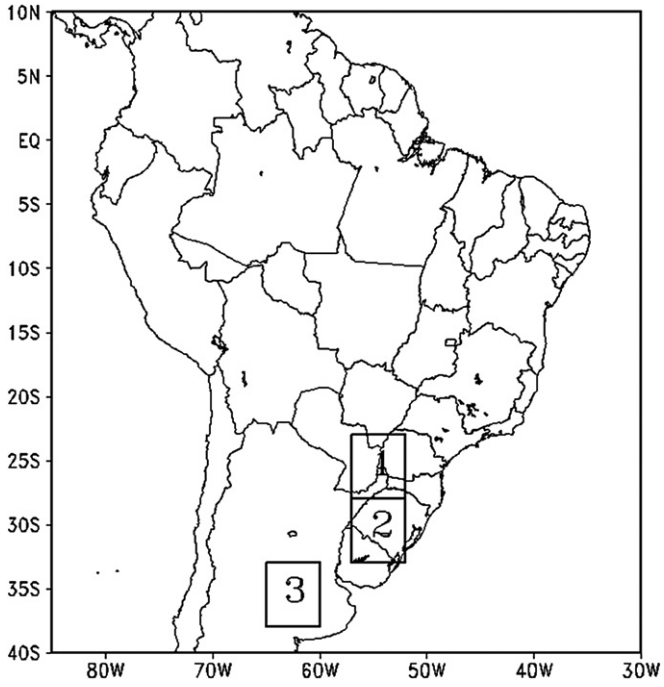

Fig. 1. Areas of analysis: area 1 (52°W–57°W, 23°S–28°S), area 2 (52°W–57°W, 28°S–33°S) and area 3 (65°W–60°W, 33°S–38°S).

The model used to investigate the present and future cold air intrusions was the Coupled Atmospheric and Oceanic Global Circulation Model (AOGCM) from CMIP-3 integrations GFDL-CM2.0 (Geophysical Fluid Dynamics Laboratory/NOAA). The resolution of the land and atmospheric components is 2° latitude–2.5° longitude; and the atmospheric model has 24 vertical levels. The ocean resolution is 1° in latitude and longitude, with meridional resolution equatorward of 30° becoming progressively finer, such that the meridional resolution is 1/3° at the equator. There are 50 vertical levels in the ocean, with 22 evenly spaced levels. More GFDL-CM2.0 information is found in Delworth et al. (2006). For the future climate, the experiment with SRES A2 scenario was taken from CMIP3 GFDL-CM2.0 from May to September 2081–2100.

Several tests were conducted to define a criterion to select the cases, and after analyzing the temperatures that normally occur in cases of cold air intrusion in each of the three areas, the criterion was based on temperature intervals, specific for each area (subtropical and extratropical regions). The mean spatial temperature for each area (considering the stations or the grid points inside a 5° lat × 5° long area) had to lie in the intervals: $T < 0$ °C; 0 °C $<= T < 2.5$ °C; 2.5 °C $<= T < 5$ °C for area 1; $T < 0$ °C; 0 °C $<= T < 2.5$ °C for area 2; and $T < 0$ °C for area 3. After applying this criterion, the cases were selected with a minimum of 4 days apart. The criterion based on a 2.5 °C temperature is commonly used as a frost reference in tropical regions (Pezza and Ambrizzi, 2005). For each group, daily composites were made for the first day of the event; and different variables were employed for the mean and the anomaly field analysis. The selected variables were SLP, zonal and meridional wind and temperature.

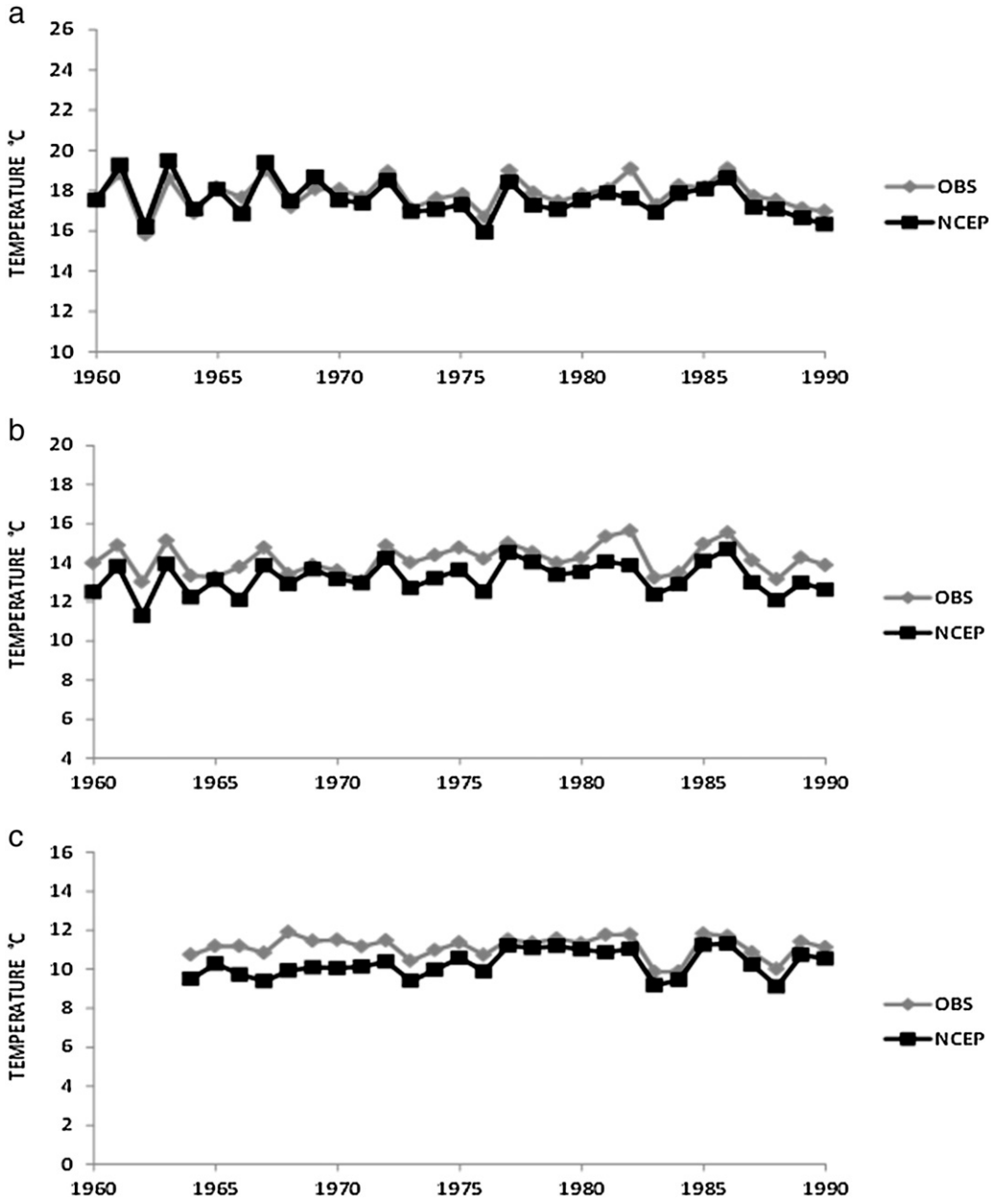

Fig. 2. Interannual spatial and temporal (May to September) mean observed temperature at surface stations and NCEP/NCAR reanalysis at 925 hPa in area 1 (a), area 2 (b) and area 3 (c).

Composites anomalies were calculated with respect to the climatological periods.

3. Results

3.1. Evaluation of model temperatures

The interannual (May–September) variability of temperature observed in meteorological stations, NCEP/NCAR reanalysis and GFDL model results is analyzed in Figs. 2–3 for each area. The timeseries of 925 hPa temperature reanalysis are in accordance with the variability of observed data in area 1 (Fig. 2a) and 2 (Fig. 2b). As regards area 3, a large agreement is noticed after 1975 (Fig. 2c). Therefore, the reanalysis temperature was used to choose the cases of cold air intrusions over southeastern South America, and to compare the reanalysis with the model results at 925 hPa. Mean temperature timeseries at 925 hPa simulated by GFDL model and those based on the reanalysis are illustrated in Fig. 3. In area 1 (Fig. 3a), GFDL overestimates the observed temperatures for most years. However, in several years, the model simulates the observed temperatures. In area 2 (Fig. 3b), a few years of underestimated temperatures are noticed and in area 3 the model underestimates the observed temperature almost in the whole period (Fig. 3c). These results are consistent with Knutson et al. (2006) who reported, for the same model, that simulations in the period of 1871 to 2000 somehow tend to warm less (more) than observations, particularly in the southern extratropics (tropics).

This subjective analysis is reflected objectively in Table 1. In area 1, the temperatures at 925 hPa from reanalysis vary from 16 °C to 19.5 °C during May–September, and average 17.6 °C (Table 1). GFDL represents the minimum value of 16 °C, as in the reanalysis, and the maximum value of 22 °C, with an average of 19.3 °C (Table 1). As for

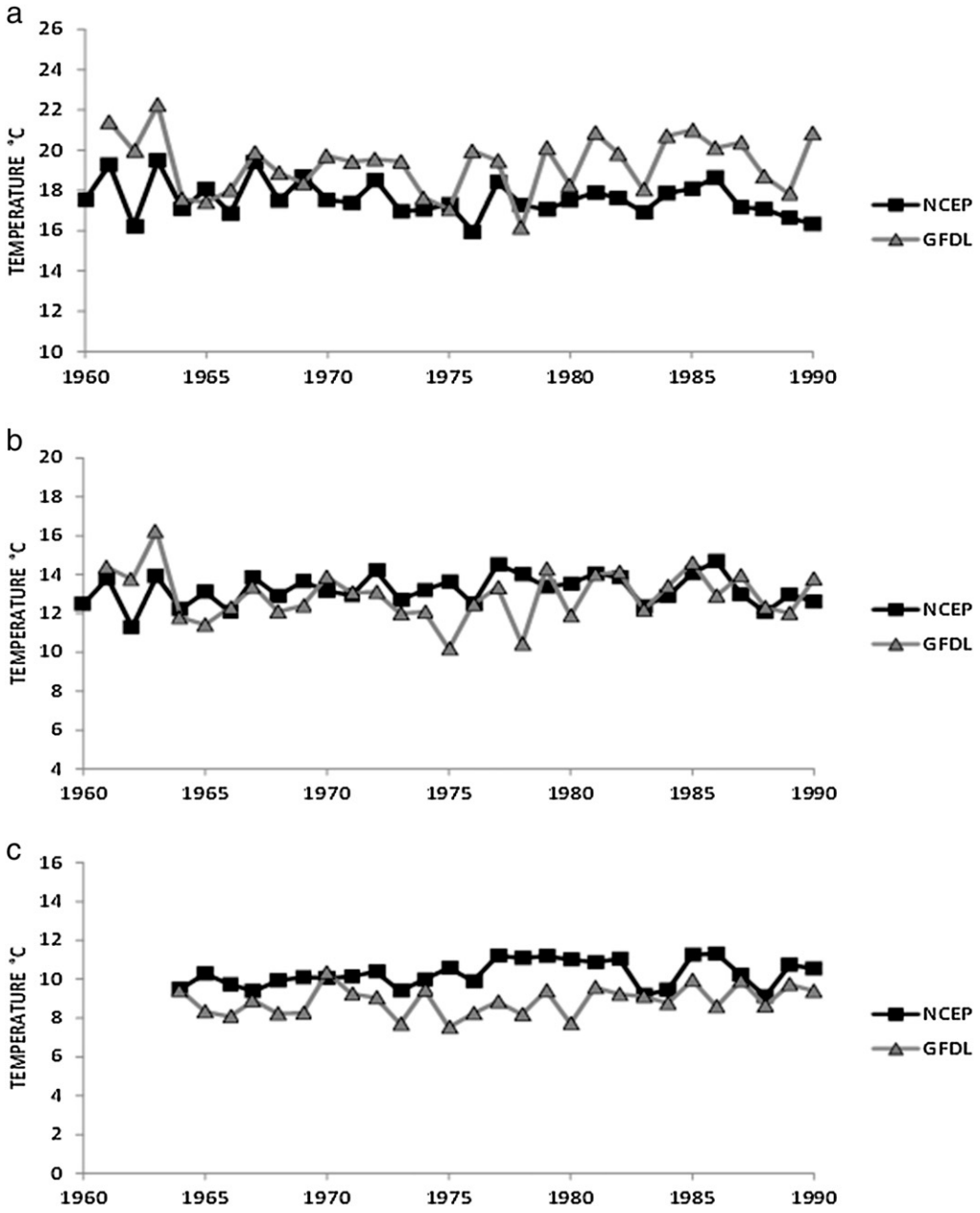

Fig. 3. Interannual spatial and temporal (May to September) mean temperature of NCEP/NCAR reanalysis and of GFDL model at 925 hPa in areas 1 (a), 2 (b) and 3 (c).

area 2, the temperatures at 925 hPa range from 11 °C to 15 °C, with an average of 13.3 °C, in the reanalysis. GFDL simulates temperatures between 10 °C and 16 °C, with an average of 12.9 °C (Table 1). In area 3, the mean values oscillate between 9 °C and 10 °C, with an average of 10.3 °C for NCEP (Table 1). GFDL results reveal temperatures between 8 °C and 11 °C, with an average of 9 °C (Table 1). Therefore, in average, the GFDL model tends to be warmer (colder) at lower (higher) latitudes. The same table shows that for the future climate, the model projects an increase of average temperature in the three areas, but in area 1 the warming is larger compared to the others.

The BIAS of model vs. reanalysis is not of the same order in every month of the period under study, i.e., May to September, with an RMSE that varies in each region depending on the month (Table 2). The BIAS sign of GFDL vs. NCEP shows such variation, depending on the area and the month. In area 1, the BIAS yields a positive (negative) value during June to September (May), thereby indicating that GFDL overestimated (underestimated) NCEP. Regarding area 2, during May to July (August and September) GFDL underestimated (overestimated) NCEP; whereas in area 3, the model underestimated the reanalysis from May to August and overestimated in September. The model represents reasonably well the interannual variability, mainly in area 2.

Table 1
Spatial mean temperature at 925 hPa from May to September.

	Area 1	Area 2	Area 3
NCEP	17.6	13.3	10.3
GFDL	19.3	12.9	9.0
GFDL future	23.2	15.3	11.1

Table 2
NCEP vs. GFDL.

Month	RMSE	BIAS
Area 1		
May	3.0	−0.2
June	2.9	0.5
July	3.3	2.0
August	3.9	3.2
September	2.5	1.3
Area 2		
May	4.2	−2.9
June	3.4	−1.3
July	2.9	−0.4
August	2.3	1.1
September	1.9	1.0
Area 3		
May	4.7	−4.1
June	3.6	−2.0
July	3.1	−1.2
August	1.7	−0.1
September	2.1	0.9

In the other areas, although there are periods of overestimation (area 1) and underestimation (area 3), there are some years with similar temperatures. Table 3 also shows that the bias is small in some months.

The annual cycle of temperature in each area shows similar behavior in areas 2 and 3, a slight overestimation of temperature in the second semester and a larger underestimation during the first semester (Fig. 4b,c). In area 1 the temperatures are very well simulated from February to May and overestimated from June to January (Fig. 4a). Thus, the model simulates the monthly temperature variations during the period of analysis, May to September.

3.2. Frequency distribution of temperature in the present and future climate

Histograms of spatial average of daily temperature from May to September are analyzed in the three areas using reanalysis, observations and the GFDL model for present and future climate (Figs. 5, 6 and 7 respectively). The reanalysis represents well the most frequent temperature intervals in areas 1 and 2, but underestimates in area 3 (Fig. 5). The frequency distribution according to GFDL shows larger number of extremes (in both tails) than observation does in every studied area, except in area 3 for the highest temperatures (Fig. 6).

The model underestimates the most frequent range of temperatures, i.e., towards the center of the histogram in the 3 areas. This result is congruent with that provided in Fig. 3 for the interannual variability of GFDL vs. NCEP temperatures in areas 2 and 3. However in area 1, the model overestimates the annual mean reanalysis temperature (Fig. 3a). The reason for this apparent inconsistency is explained by the magnitude of the frequency at which the highest temperatures of the GFDL model are above those of the observations, which are similar to NCEP (Figs. 5a, 6a). Even though GFDL also overestimates the observed frequency of the highest temperatures in area 2 (Fig. 6b), the proportion is considerably smaller than for area 1. Towards the other end of the histogram, GFDL overestimates observed lower temperatures, mainly in area 2 (Fig. 6).

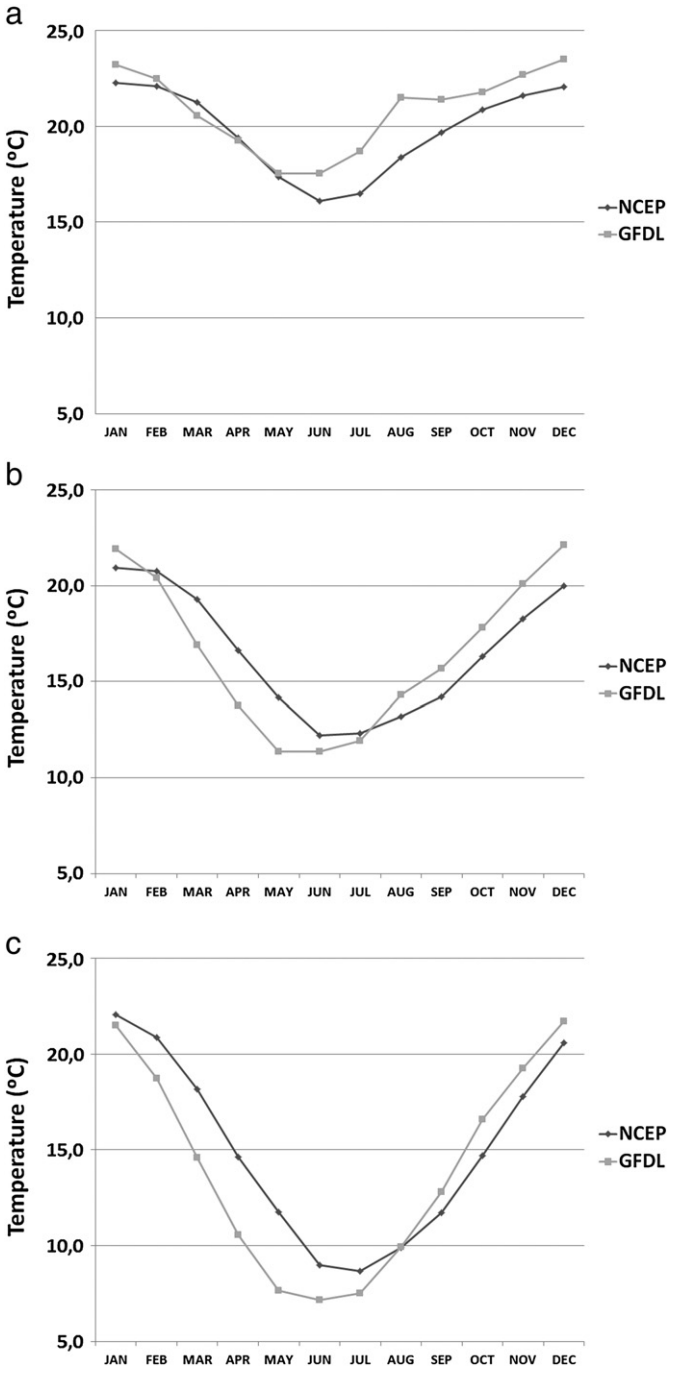

Fig. 4. Annual cycle of spatial mean temperature of NCEP/NCAR reanalysis and of GFDL model at 925 hPa in areas 1 (a), 2 (b) and 3 (c).

Table 3
Number of cases from May to September (the whole period).

		T < 0 °C	2.5 °C < T ≤ °0 °C	2.5 °C ≤ T < 5 °C
Area 1	Reanalysis	1	1	16
	GFDL present	2	12	39
	GFDL future	0	0	7
Area 2	Reanalysis	1	25	
	GFDL present	29	87	–
	GFDL future	0	12	–
Area 3	Reanalysis	30		
	GFDL present	103	–	–
	GFDL future	16	–	–

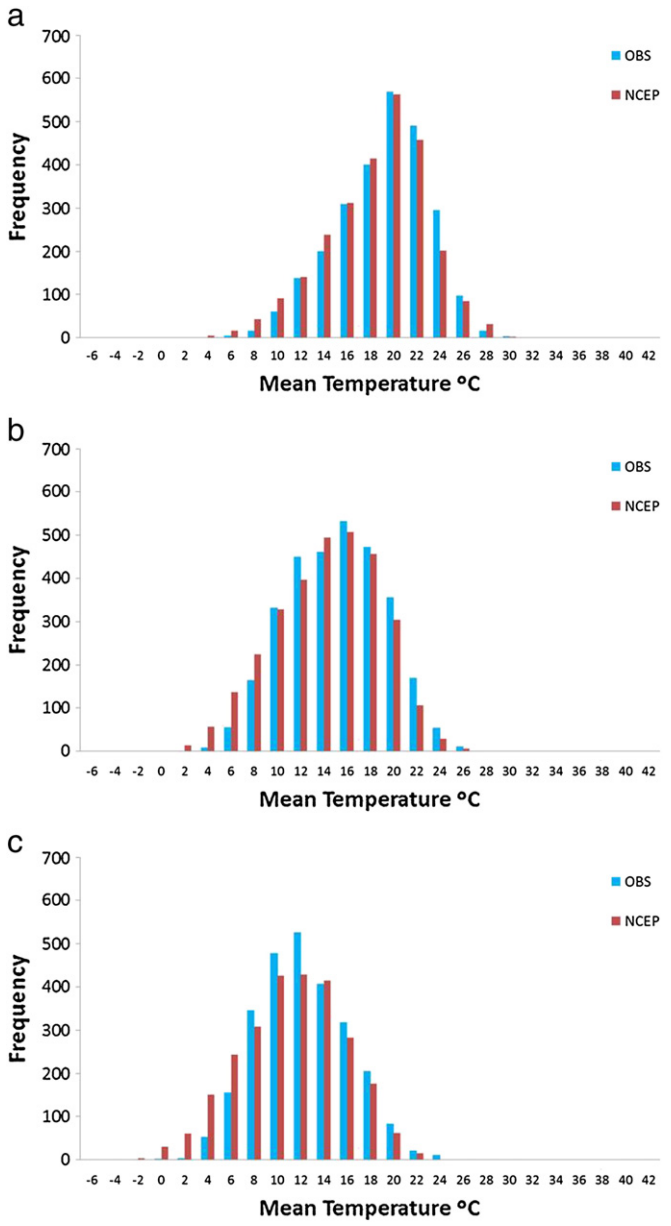

Fig. 5. Histograms of spatial mean temperature in areas 1 (a), 2 (b) and 3 (c) for the period of 1964 to 1980. Blue columns represent observations and red columns represent NCEP/NCAR reanalysis.

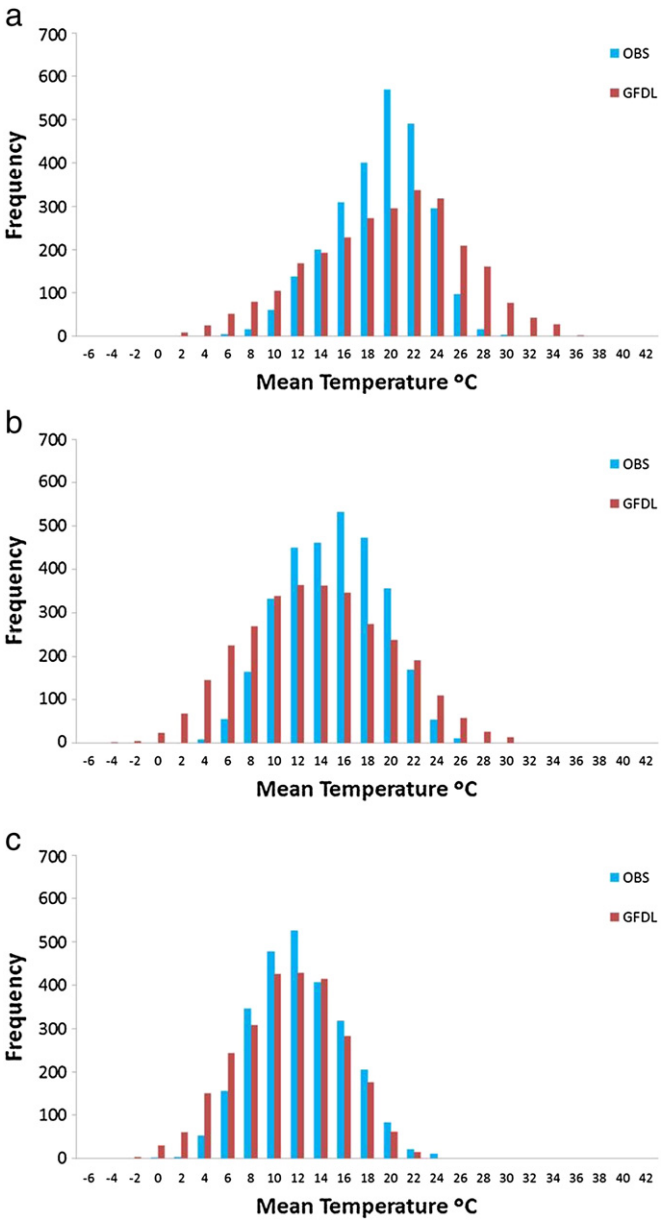

Fig. 6. Histograms of spatial mean temperature in areas 1 (a), 2 (b) and 3 (c) for the period of 1964 to 1980. Blue columns represent observations and red columns represent GFDL model.

The frequency distribution of temperature according to the GFDL model in the present versus future is displayed in Fig. 7. Comparing the frequency distribution of future with respect to present climate, the three areas of study show that the frequency distribution shifts towards higher temperatures, which is consistent with the global warming. This displacement is greater in area 1 if compared to areas 2 and 3. In area 1, the maximum frequency of occurrence in the present climate is 22 °C, while, for the future, that maximum is 26 °C (Fig. 7a). Area 2 displays the highest frequency of occurrence around 12 °C and 14 °C, while for the future is 14 °C. Yet temperature frequency above this threshold increases in the future in relation to the present (Fig. 7b). In area 3, the maximum frequency occurs for temperatures of 10 °C in the present and 12 °C in the future (Fig. 7c) and higher temperatures are more common in the future than in the present. As a matter of fact, below these respective threshold values in each area, the temperature frequencies of occurrence are significantly lower in the future than in the present climate. Consequently, the frequency of occurrence of cold air intrusion is substantially reduced in the future in all areas.

3.3. Frequency of cold air intrusions in the present and future climate

This section deals with the frequency of cold air intrusions from May to September in the three areas using the model and reanalysis results. The frequencies are analyzed in each temperature interval of each area (Tables 3 and 4).

Three temperature intervals were analyzed in area 1 (Table 3), since temperatures are higher in this region than in the other two regions located at higher latitudes. In this area, only one case of temperature below zero was detected in the reanalysis and 2

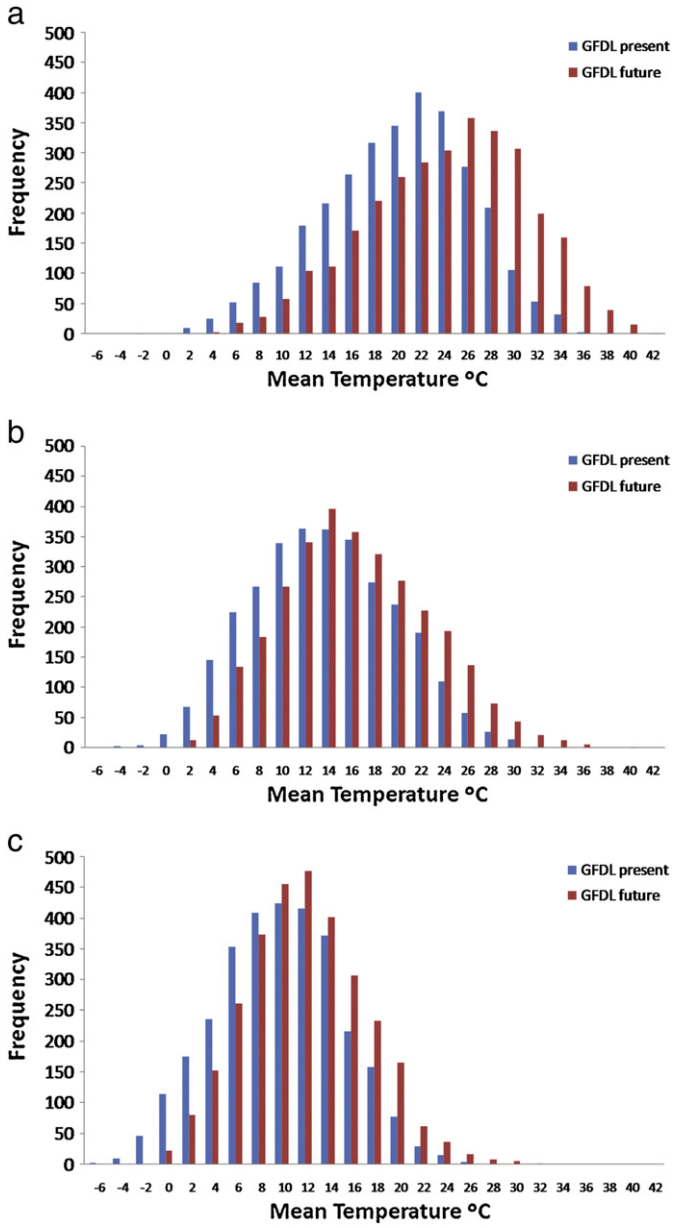

Fig. 7. Histograms of spatial mean temperature in areas 1 (a), 2 (b) and 3 (c). Blue columns represent GFDL results for the period of 1961–1990 and red columns represent GFDL results for the future climate (2081–2100).

cases in GFDL model results. In the 0 °C–2.5 °C interval, one case was identified in the reanalysis while GFDL showed 12 cases. With respect to the 2.5 °C–5 °C interval, the number of cases increased in the reanalysis to 16 and to 39 in GFDL, respectively. Therefore, in area 1, the models simulated a higher frequency of cases than observations did, taking into account that the reanalysis was very close to the observed data. In the future climate projection, no cases of spatial average temperature below 2.5 °C were detected in area 1 from May to September. In this area, the minimum extreme temperature interval in the future climate simulation was registered between 2.5 °C and 5 °C. In such interval, 7 cases were identified in a 20-year period. The frequency was reduced from 1.3 cases/year in the control climate to 0.4 cases/year in the future climate projections (Table 4).

Table 4
Frequency of cases from May to September.

	Area 1 (2.5 °C ≤ T < 5 °C)	Area 2 (2.5 °C < T ≤ 0 °C)	Area 3 (T < 0 °C)
NCEP	0.5/year	0.8/year	1/year
GFDL	1.3/year	2.9/year	3.4/year
GFDL future	0.4/year	0.6/year	0.8/year

With regard to area 2, two temperature intervals were analyzed (Table 3). Only one case occurred with temperatures below zero in the reanalysis, while GFDL simulates 29 cases. In the 0 °C–2.5 °C interval, the number of cases increased in the reanalysis and model results, and the model also simulated a higher number of cases than observations did. In this area, no cases of temperature below 0 °C were detected in the future climate projections. In the 0 °C–2.5 °C interval, there were 12 cases in 20 years, with a frequency of 0.6 cases/year, less than the frequency of the control period 2.9 cases/year (Table 4).

As it could be expected from area 3, the frequency of cold air intrusions with temperatures below zero is higher in this area than in the other two (Table 3). The number of cases is also greater in GFDL than in the reanalysis. As for the future climate projection, the number of cases decreased to 16 in 20 years. Thus, the frequency changed from 3.4 cases/year in the control to 0.8 cases/year in the future (Table 4).

The results in Table 3 are in line with the analysis in Fig. 6, which shows that the GFDL model overestimates observations regarding to the number of low temperature cases. This is clearly reflected in the number of cold air intrusions, yielding substantially higher values for areas 2 and 3 in different selected intervals. Moreover, the results discussed above for the future climate (Fig. 7) are confirmed in Table 3, where the number of cold air intrusion cases decreases significantly to the point of not showing future events. That is the case of area 1 at intervals of less than 2.5 °C and area 2 for the interval below 0 °C. With respect to area 3, being further south, temperature values even below 0 °C are obtained; however, the frequency of cases in the future decreases significantly compared to the present.

3.4. Mean atmospheric characteristics in the present and future climate in cases of cold air intrusion

The large-scale characteristics associated with cases of cold air intrusions resulting from GFDL model for the present climate as compared to those obtained from NCEP reanalysis were analyzed. The atmospheric characteristics represented by the model in the present and future climate were analyzed in composites of cases identified in each region. As the number of cases is smaller in the future projections than in the present climate (Table 3), the smallest number was taken for the two periods in each area. The limited number for the present climate was selected by the smallest temperatures for each interval of the three areas. The composites were performed with 7 cases identified in area 1 in the 2.5 °C–5.0 °C interval; 12 cases identified in area 2 in the 0 °C–2.5 °C interval, and 16 cases identified in area 3 with temperatures below 0 °C. The patterns resulting from the composites of these events are displayed in Fig. 8 for the reanalysis and Figs. 9, 10, and 11 for the GFDL model.

The resulting patterns of the Sea Level Pressure (SLP), temperature and wind fields at 925 hPa simulated by the model (Figs. 9–11 upper row) are similar to the results obtained from the reanalysis in the different areas (Fig. 8). The results agree with previous studies of Garreaud (2000), Vera and Vigliarolo (2000), Müller and Berri (2007), and Müller and Berri (2012). The simulated pressure values (Fig. 9a) are generally of the same order as those from the reanalysis (Fig. 8a) as well as SLP anomalies that appear well represented in the areas under study.

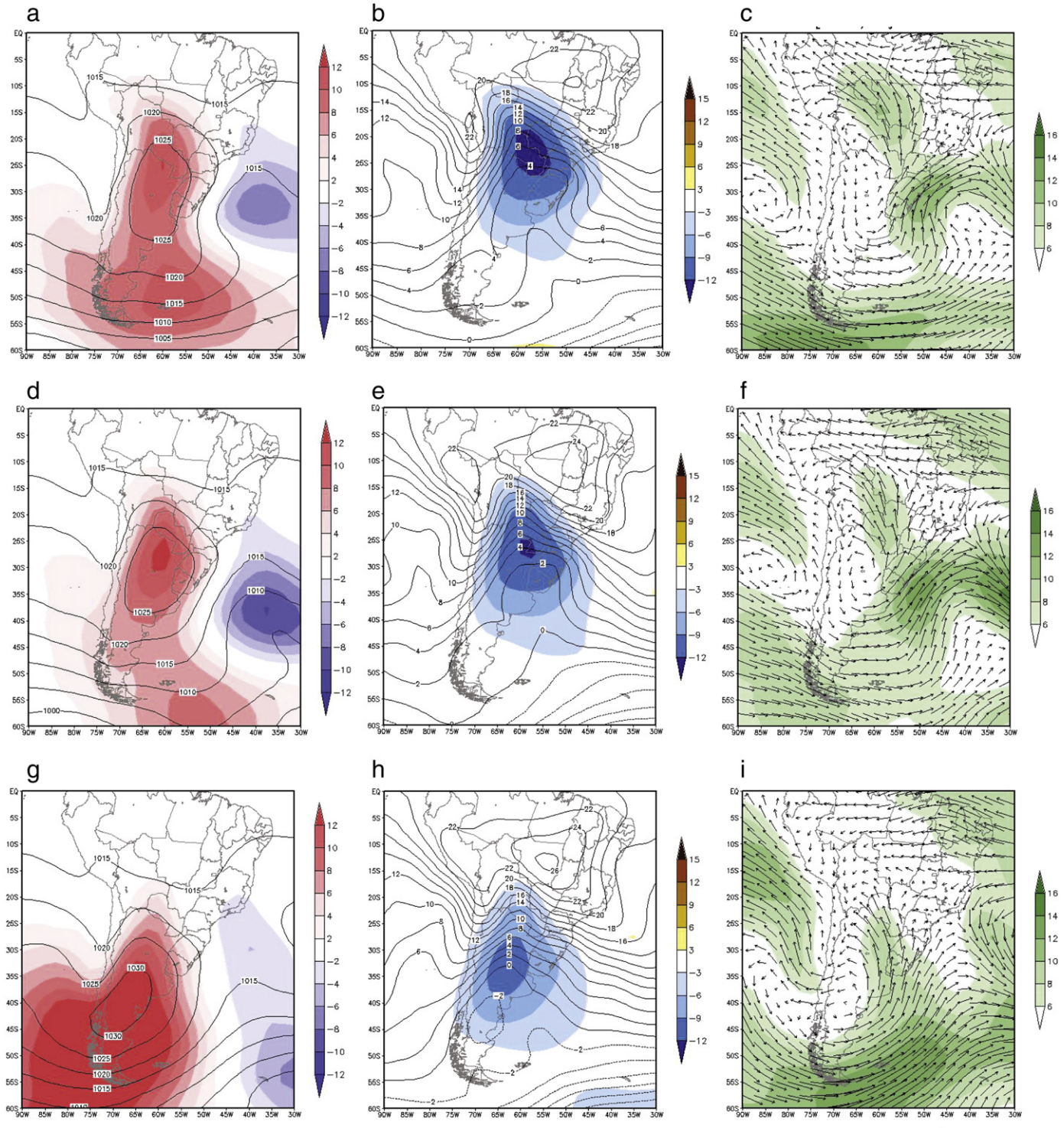

Fig. 8. Composites of NCEP/NCAR reanalysis cases with spatial mean temperature between 2.5 °C and 5.0 °C in area 1 (a–c), 0 °C and 2.5 °C in area 2 (d–f) and temperature bellow 0 °C in area 3. SLP and anomalies (a,d,g), 925 hPa temperature and anomalies (b,e,h), 925 hPa wind vector and magnitude (c,f,i).

On the other hand, when comparing the GFDL model results of both periods (present and future), the pressure values are similar for both of them, but the anomalies extend to lower latitudes in the future climate and are more intense in the analyzed areas (Fig. 9a,d for area 1; Fig. 10a,d for area 2, and Fig. 11a,d for area 3). The SLP field for area 1 presents a high pressure center over northern Argentina yielding maximum values of 1030 hPa in the present climate, which is consistent with the cold air intrusions (Fig. 9a). In the future composite, this center extends to Paraguay, Uruguay and southern Brazil (Fig. 9d). Anomalies of 12 hPa over northern Argentina, in the control, extend to lower latitudes as well. The maximum pressure associated with the cold air intrusion in area 2 is 1025 hPa in the control (Fig. 10a) and increases to 1030 hPa in the composite of the future projection

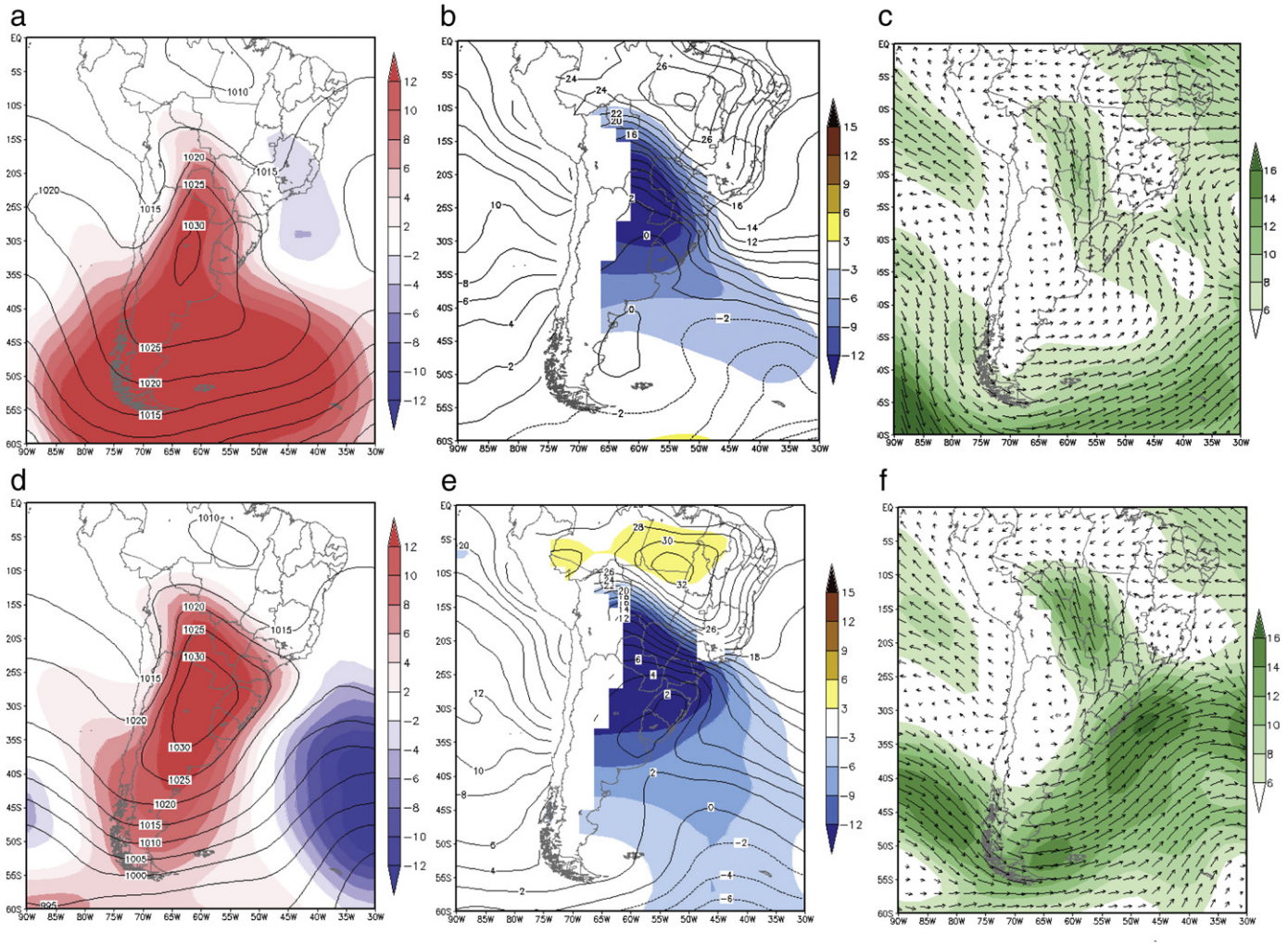

Fig. 9. Composites of cases with spatial mean temperature between 2.5 °C and 5.0 °C in area 1 for GFDL [1961–1990] (above) and future climate [2081–2100] (below) of SLP and anomalies (a,d), 925 hPa temperature and anomalies (b,e), 925 hPa wind vector and magnitude (c,f).

(Fig. 10d). Anomalies of 12 hPa over southeastern Argentina, in the control, also expand to Paraguay, Uruguay and southern Brazil in the future projection. The center of high pressure composite for area 3 in the control has a maximum value of 1025 hPa over southern Argentina and southern Chile (Fig. 11a). In the future, the maximum value of high pressure is 1030 hPa and the high pressure anomalies extend over lower latitudes of Argentina (Fig. 11d).

Figs. 9b, 10b and 11b show that the simulated isotherms better represent the reanalysis (Fig. 8) in areas 2 and 3 rather than area 1. In the future scenario (Figs. 9e, 10e and 11e), more intense temperature anomalies are projected over South America than in the present climate. Negative temperature anomalies extend to lower latitudes far beyond the composites of the present climate, implying stronger gradients. The composites for area 1 reveal the expansion of negative temperature anomalies from the control to the future climate projections, but also a temperature increase in Amazonia, from 28 °C in the control to 32 °C in the future climate (Fig. 9b,e). Negative anomalies intensify for the composite of area 2 in the future projection and also the north–south gradient (Fig. 10b,e). With respect to area 3, the temperature gradient also increases and anomalies of −6 °C exist in large areas of Argentina in the present (Fig. 11b), while anomalies of −9 °C extend to these areas in the future (Fig. 11e).

The 925 hPa wind fields present confluence over the ocean close to South America (Fig. 8c), demonstrating the influence of frontal systems on the cold air intrusion of the three cases, also represented by the model (Figs. 9c, 10c, 11c). In the future, the southerly flow is stronger and reaches lower latitudes than it does in the present time (Figs. 9f, 10f, 11f).

4. Conclusion

This paper aimed to investigate the coupled GFDL-CM2.0 model ability to simulate the frequency of cold air intrusions in the present climate as well as the changes in the frequency of occurrence and atmospheric characteristics in a future climate scenario.

The average temperature of the reanalysis is overestimated (underestimated) by the GFDL model in area 1 (areas 2 and 3) because the proportion of temperature frequency in the range of the highest temperatures is considerably higher (lower) for the GFDL model. Nevertheless, the GFDL model overestimated the number of cold air intrusions over southeastern South America in the period 1961–1990 in the three regions.

Conversely, the frequency distribution of the spatial mean temperature in the three areas from the GFDL present climate is displaced to the right in the future (to higher temperatures), which is consistent with the global warming and indicates extremes shifting to higher

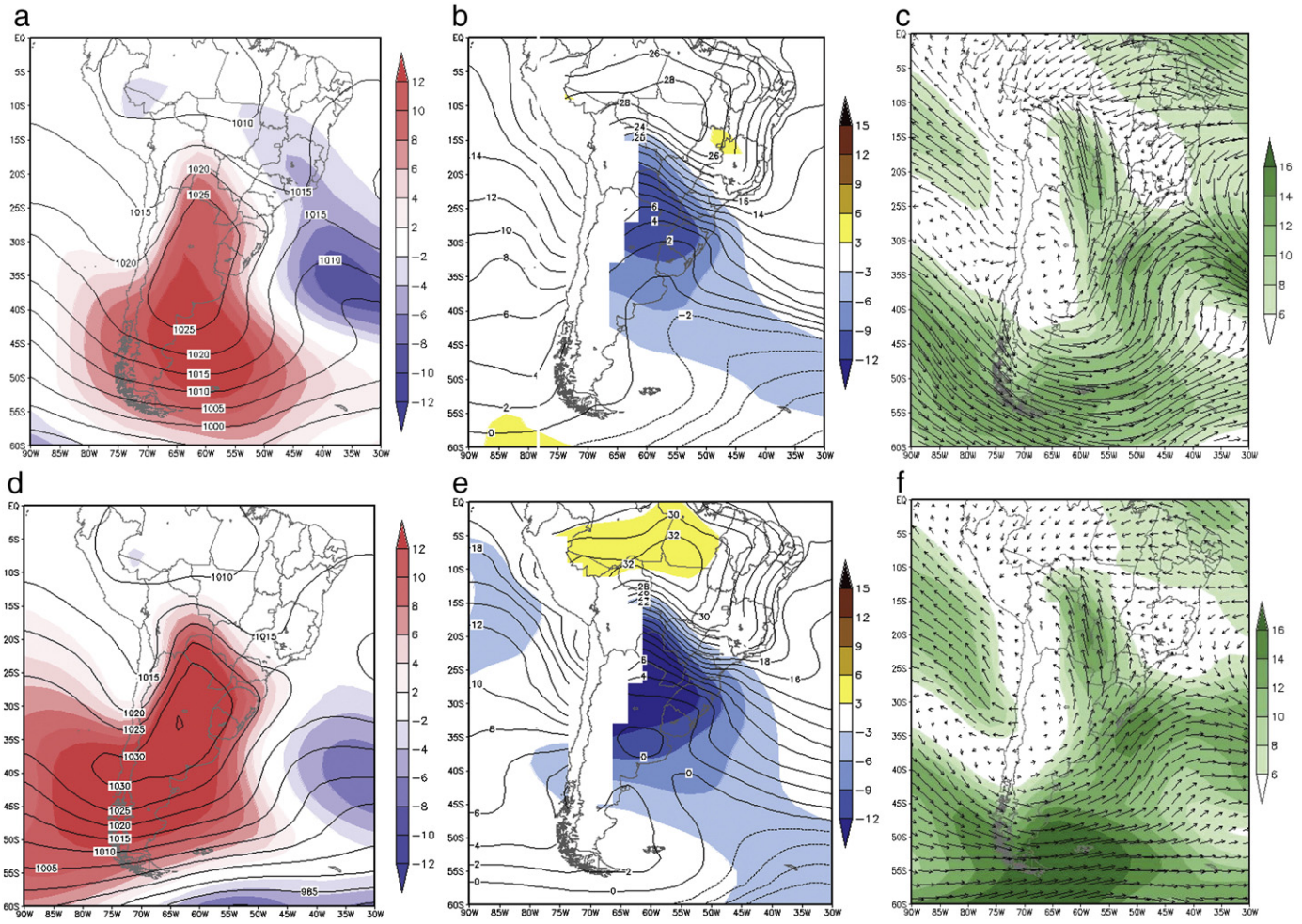

Fig. 10. Composites of cases with temperature between 0 °C and 2.5 °C in area 2 for GFDL [1961–1990] (above) and future climate [2081–2100] (below) of SLP and anomalies (a,d), 925 hPa temperature and anomalies (b,e), 925 hPa wind vector and magnitude (c,f).

temperatures. In these areas, a smaller number of cases are simulated by GFDL in the future projections in the three areas of southeastern South America affected by frosts in the cold season of the present climate. Even area 1 does not present any event in the future with temperatures below 2.5 °C, and, area 2, below 0 °C.

The model represents well the configurations of atmospheric fields in the composites of the three areas. Comparing the atmospheric features simulated in the present and future periods, an increase in the temperature gradient can be noticed over South America, which is associated with warming in tropical South America, stronger cold air intrusion and to the fact that the cold air reaches lower latitudes in the future climate than it does in the present climate. The high pressure centers related to the intrusions are also more intense and the temperature anomalies are stronger in the future than they are in the present, mainly in areas 2 and 3.

Indeed, an extended cold air intrusion in subtropical areas of South America is simulated in the future projections compared to the present climate simulation. However, fewer cases of cold air are simulated in the defined threshold intervals in the future projections. The apparent inconsistency is related to the same threshold intervals applied to the present and future when the mean temperature has changed. Thus, even in a future scenario when the mean temperature will be higher than it is in the present and when a reduced number of cold air intrusions with the defined temperature threshold is projected to occur, the systems would be more intense and the cold air would reach lower latitudes in a stronger temperature gradient environment. The future projections of fewer cold air intrusions over southeastern South America but more intense systems featuring stronger negative anomalies in the future climate would produce a strong impact on agriculture.

Acknowledgments

The authors acknowledge the support from Projects PICT-PRH 0023 (FONCYT, Argentina) and Prosul 490466/2006-0 (CNPq, Brazil). IFAC thanks CNPq and FAPESP for research support. The authors would also like to thank the international modeling groups for providing their data for analysis, the Program for Climate Model Diagnosis and Intercomparison (PCMDI) for collecting and archiving the model data, the JSC/CLIVAR Working Group on Coupled Modeling (WGCM) and their Coupled Model Intercomparison Project (CMIP) and Climate Simulation Panel for organizing the model data analysis activity and the IPCC WG1 TSU for technical support. The IPCC Data Archive at Lawrence Livermore National Laboratory is supported by the Office of Science, U.S. Department of Energy.

References

Alexander, L.V., Zhang, X., Peterson, T.C., Caesar, J., Gleason, B., Klein Tank, A.M.G., Haylock, M., Collins, D., Trewin, B., Rahimzadeh, F., Tagipour, A., Ambenje, P., Rupa Kumar, K., Revadekar, J., Griffiths, G., Vincent, L., Stephenson, D., Burn, J., Aguilar, E., Brunet, M., Taylor, M., New, M., Zhai, P., Rusticucci, M., Vazquez-Aguirre, J.L., 2006. Global

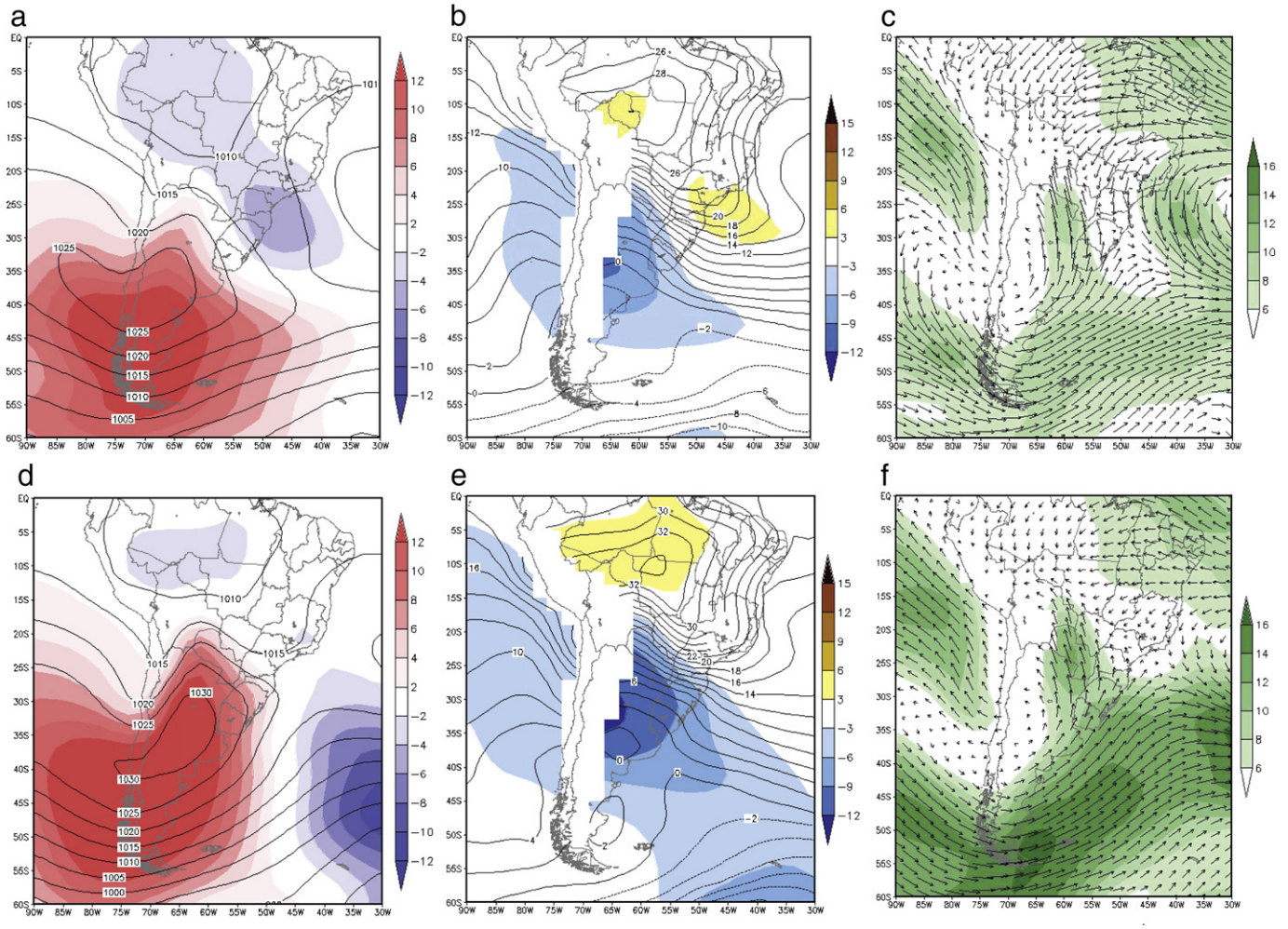

Fig. 11. Composites of cases with temperature bellow 0 °C in area 3 for GFDL present climate [1961–1990] (above) and future climate [2081–2100] (below) of SLP and anomalies (a,d), 925 hPa temperature and anomalies (b,e), 925 hPa wind vector and magnitude (c,f).

observed changes in daily climate extremes of temperature and precipitation. J. Geophys. Res. 111, D05109. http://dx.doi.org/10.1029/2005JD006290.

Andrade, K.M., Müller, G.V., Cavalcanti, I.F.A., Fernandéz Long, M.E., Bidegain, M., Berri, G.J., 2012. Avaliação de mudanças na freqüência de sistemas frontais sobre o Sul da América do sul em projeções do clima futuro. Meteorológica 37 (1), 15–26 (http://www.cenamet.org.ar/archivos/Vol37-Nro1-2012.pdf).

Barrucand, M., Rusticucci, M., Vargas, W., 2008. Temperature extremes in the south of South America in relation to Atlantic Ocean surface temperature and southern hemisphere circulation. J. Geophys. Res. 113, D20111. http://dx.doi.org/10.1029/2007JD009026.

Bonsal, B.R., Zhang, X.L., Vincent, A., Hogg, W.D., 2001. Characteristics of daily and extreme temperatures over Canada. J. Climate 14, 1959–1976.

Delworth, T., et al., 2006. GFDL's CM2 global coupled climate models — part 1: formulation and simulation characteristics. J. Climate 19 (5), 643–674.

Easterling, D.R., 2002. Recent changes in frost days and the frost-free season in the United States. Bull. Am. Meteorol. Soc. 83, 1327–1332.

Easterling, D.R., Meehl, G.A., Parmesan, C., Changnon, S.A., Karl, T.R., Mearns, L.O., 2000. Climate extremes: observations, modeling, and impacts. Science 289 (5487), 2068–2074.

Fernández Long, M.E., Müller, G., 2006. Annual and monthly trends in frost days in the Wet Pampa. Proceeding 8th International Conference on Southern Hemisphere Meteorology and Oceanography, Foz do Iguazú, Brasil, pp. 249–253.

Fernandez Long, M.E., Müller, G.V., Beltrán-Przekurat, A., Scarpati, O., 2013. Long-term and recent changes in temperature-based agroclimatic indices in Argentina. Int. J. Climatol. 33 (7), 1673–1686.

Garreaud, René, 2000. Cold air incursions over subtropical South America: mean structure and dynamics. Mon. Weather Rev. 128, 2544–2559.

Hall, N., Hoskins, B., Valdes, P., Senior, C., 1994. Storm tracks in a high resolution GCM with doubled carbon dioxide. Q. J. R. Meteorol. Soc. 120, 1209–1230.

Haylock, M.R., Peterson, T., Abreu de Sousa, J.R., Alves, L.M., Ambrizzi, T., Baez, J., Barbosa de Brito, J.I., Barros, V.R., Berlato, M.A., Bidegain, M., Coronel, G., Corradi, V., Garcia, V.J., Grimm, A.M., Jaildo dos Anjos, R., Karoly, D., Marengo, J.A., Marino, M.B., Meira, P.R., Miranda, G.C., Molion, L., Muncunil, D.F., Nechet, D., Ontaneda, G., Quintana, J., Ramirez, E., Rebello, E., Rusticucci, M., Santos, J.L., Varillas, I.T., Vincent, L., Yumiko, M., 2006. Trends in total and extreme South American rainfall 1960–2000 and links with sea surface temperature. J. Climate 19, 1490–1512.

IPCC, 2007. Intergovernmental panel on climate change. In: Core Writing Team, Pachauri, R.K., Reisinger, A. (Eds.), Contribution of Working Groups I, II and III to the Fourth Assessment Report of the Intergovernmental Panel on Climate Change. IPCC, Geneva, Switzerland (104 pp.).

Kalnay, E., et al., 1996. The NCEP/NCAR 40-year reanalysis project. Bull. Am. Meteorol. Soc. 77, 437–471.

Knutson, T.R., Delworth, T.L., Dixon, K.W., Held, I.M., Lu, J., Ramaswamy, V., Schwarzkopf, M.D., Stenchikov, G., Stouffer, R.J., 2006. Assessment of twentieth century regional surface temperature trends using the GFDL CM2 coupled models. J. Climate 19 (9), 1624–1651.

Kushner, P.J., Held, I., Delworth, M.T.L., 2001. Southern hemisphere atmospheric circulation response to global warming. J. Climate 14, 2238–2249.

Marengo, J., Camargo, C.C., 2008. Surface air temperature trends in Southern Brazil for 1960–2002. Int. J. Climatol. 28, 893–904. http://dx.doi.org/10.1002/joc.1584.

Marengo, J.A., Rusticucci, M., Penalba, O., Renom, M., 2010. An intercomparison of observed and simulated extreme rainfall and temperature events during the last half of the twentieth century: part 2: historical trends. Clim. Chang. 98, 509–529. http://dx.doi.org/10.1007/s10584-009-9743-7.

Meehl, G., Zwiers, F., Evans, J., Knutson, T., Mearns, L., Whetton, P., 2000. Trends in extreme weather and climate events: issues related to modeling extremes in projections of future climate change. Bull. Am. Meteorol. Soc. 81, 427–436.

Menzel, A., Jakobi, G., Ahas, R., Scheifinger, H., Estrella, N., 2003. Variations of the climatological growing season (1951–2000) in Germany compared with other countries. Int. J. Climatol. 23, 793–812. http://dx.doi.org/10.1002/joc.915.

Müller, G.V., Berri, G.J., 2007. Atmospheric circulation associated with persistent generalized frosts in central-southern South America. Mon. Weather Rev. 135 (4), 1268–1289.

Müller, G.V., Berri, G.J., 2012. Atmospheric circulation associated with extreme generalized frosts persistence in central-southern South America. Clim. Dyn. 38 (5–6), 837–857. http://dx.doi.org/10.1007/s00382-011-1113-2.

Pezza, A.B., Ambrizzi, T., 2005. Dynamical conditions and synoptic tracks associated with different types of cold surges over tropical South America. Int. J. Climatol. 25, 215–241.

Rusticucci, M., Renom, M., 2008. Variability and trends in indices of quality-controlled daily temperature extremes in Uruguay. Int. J. Climatol. 28, 1083–1095.

Rusticucci, M., Marengo, J., Penalba, O., Renom, M., 2010. Anintercomparison of model-simulated in extreme rainfall and temperature events during the last half of the twentieth century. Part 1: mean values and variability. Clim. Chang. 98, 493–508. http://dx.doi.org/10.1007/s10584-009-9742-8.

Salinger, M.J., Griffiths, G.M., 2001. Trends in New Zealand daily temperature and rainfall extremes. Int. J. Climatol. 21, 1437–1452.

Skansi, M.L., Brunet, M., Sigró, J., Aguilar, E., Groening, J.A.A., Bentancur, O.J., Yaruska Rosa Geier, C., Amaya, R.L.C., Jácome, H., Ramos, A.M., Rojas, C.O., Pastén, A.M., Mitro, S.S., Jiménez, C.V., Martínez, R., Alexander, L.V., Jones, P.D., 2013. Warming and wetting signals emerging from analysis of changes in climate extreme indices over South America. Glob. Planet. Chang. 100, 295–307.

SREX, 2012. Managing the risks of extreme events and disasters to advance climate change adaptation. In: Field, C.B., Barros, V., Stocker, T.F., Qin, D., Dokken, D.J., Ebi, K.L., Mastrandrea, M.D., Mach, K.J., Plattner, G.-K., Allen, S.K., Tignor, M., Midgley, P.M. (Eds.), A Special Report of Working Groups I and II of the Intergovernmental Panel on Climate Change. Cambridge University Press, Cambridge, UK, and New York, NY, USA (582 pp.).

Tencer, B., Rusticucci, M., Jones, P., Lister, D., 2011. A southeastern South American daily gridded dataset of observed surface minimum and maximum temperature for 1961–2000. Bull. Am. Meteorol. Soc. 92, 1339–1346.

Trenberth, K.E., 1999. Conceptual framework for changes of extremes of the hydrological cycle with climate change. Clim. Chang. 42, 327–339.

Vera, C., Vigliarolo, P.K., 2000. A diagnostic study of cold-air outbreaks over South America. Mon. Weather Rev. 128, 3–24.

Vincent, L.A., Peterson, T.C., Barros, V.R., Marino, M.B., Rusticucci, M., Carrasco, G., Ramirez, E., Alves, L.M., Ambrizzi, T., Berlato, M.A., Grimm, A.M., Marengo, J.A., Molion, L., Moncunill, D.F., Rebello, E., Anunciação, Y.M.T., Quintana, J., Santos, J.L., Baez, J., Coronel, G., Garcia, J., V.L., Trebejo, I., Bidegain, M., Haylock, M.R., Karoly, D., 2005. Observed trends in indices of daily temperature extremes in South America, 1960–2002. J Climate 18, 5011–5023.

Yin, J.H., 2005. A consistent poleward shift of the storm tracks in simulations of 21st century climate. Geophys. Res. Lett. 32, L18701. http://dx.doi.org/10.1029/2005GL023684.